RSC Advances

PAPER

View Article Online
View Journal | View Issue

Open Access Article. Published on 22 August 2024. Downloaded on 3/8/2026 10:43:55 AM.
This article is licensed under a Creative Commons Attribution-NonCommercial 3.0 Unported Licence.

Check for updates

Cite this: *RSC Adv.*, 2024, **14**, 26625

Synthesis of novel pyrazole acetals of andrographolide and isoandrographolide as potent anticancer agents†

Siva Kumar Rokkam,[a] Manohar Bhujel,[a] Dolly Jain,[c] Lakshminath Sripada,[a] Srinivas Nanduri,[b] Avinash Bajaj[c] and Nageswara Rao Golakoti*[a]

Globally, cancer is the most prevalent chronic disease-related cause of death. Although there are many anticancer drugs, some of them have adverse effects. Due to their limited side effects, natural products are preferred over synthetic drugs. Andrographolide and its derivatives are known to be potent anticancer agents. In this context, sixteen novel 3,19-(NH-3-aryl-pyrazole) acetals of andrographolide and isoandrographolide (**1a–1h**, **2a–2g**, **2i**) from 3-aryl-1-*H*-pyrazole-4-carboxaldehydes (**a–i**) were synthesized. All the synthesized compounds were characterized using ^{1}H NMR, ^{13}C NMR, HRMS, FT-IR, and UV-vis spectroscopy. All the compounds were evaluated against a panel of 60 different human cancer cell lines for their anticancer potential at NCI, USA. Four compounds, having promising GI_{50}s (50% growth inhibitory activity) on all 60-cell lines were selected for further *in vitro* studies. Out of these four compounds, compound **1g** exhibited the best IC_{50} (3.08 μM) against the colon cancer cell line, HCT-116. Cell cycle analysis, annexin V-FITC/PI, and ROS assays revealed that the apoptosis of HCT-116 cells induced by compound **1g** could be mainly attributed to the elevated levels of intracellular ROS. Further, the structure–activity relationship revealed that the pyrazole moiety of andrographolide plays a key role in their anticancer properties. These compounds were further examined for *in silico* ADMET and Lipinski characteristics to assess their potential as lead compounds.

Received 22nd January 2024
Accepted 13th August 2024

DOI: 10.1039/d4ra00547c

rsc.li/rsc-advances

1. Introduction

Andrographis paniculata (*A. paniculata*) is an annual herb and a member of the family Acanthaceae that expands up to 1–2 meters in height mostly in shady places. Due to its exceptionally bitter flavor, it is often referred to as the "King of Bitters". *A. paniculata* has a rich history in traditional medical practices in Southeast Asia, India, and China, and has been used for several generations.[1,2] Traditionally, the leaves and roots of this plant have been utilized for a variety of therapeutic purposes in Asia and Europe. In China, this plant extract is used to eliminate toxins and cool the body.[3,4] In India, it is used to cure diabetes, dysentery, herpes, jaundice, helminth infection, and ulcers, and is topically used to treat snake bites and skin infections.[5,6]

Numerous research investigations have demonstrated that *A. paniculata* extracts exhibit a plethora of pharmacological activity, including anti-cancer, anti-inflammatory, anti-viral, anti-malarial, anti-oxidant, anti-diarrheal, hepatoprotective, and immunostimulatory activities.[5–9] The observed activities of the methanolic extract are primarily attributed to the plant's major phytochemical constituent andrographolide.[10,11] The recent research findings revealed that andrographolide and its derivatives exert their anticancer effects by cell cycle arrest *via* increasing the levels of tumor suppressor proteins p53, p21 and p16, inducing apoptosis.[12–14] Andrographolide and its derivatives also suppress TNF-α, TGF-β1, IL-1β, IL-6 levels, angiogenic factor VEGF, NF-kB signaling pathway, and causes degradation of proto-oncogene tyrosine-protein kinase Src. Further, andrographolide acts as antiangiogenic and found to inhibit cell migration and invasion in A549, HT29, CT26, lovo, and cholangiocarcinoma cells by interfering with the production of proteins and cellular pathways that are crucial for the spread of cancer.[15–18]

Our previous studies on various andrographolide and isoandrographolide derivatives such as C-12-alkyl/benzyl/sulfamoyl-phenyl/amino-14-deoxyandrographolides, 3,19-benzylidene-andrographolide/isoandrographolide, 3,19-heteroaromatic acetals of andrographolide/isoandrographolide, 14-deoxy-12-hydroxy-andrographolide acetals displayed excellent

[a]Department of Chemistry, Sri Sathya Sai Institute of Higher Learning, Prasanthi Nilayam, Andhra Pradesh, India. E-mail: gnageswararao@sssihl.edu.in

[b]Department of Chemical Sciences, National Institute of Pharmaceutical Education and Research, Balanagar, Hyderabad, Telangana, 500037, India

[c]Laboratory of Nanotechnology and Chemical Biology, Regional Centre for Biotechnology, NCR Biotech Science Cluster, 3rd Milestone, Faridabad-Gurgaon Expressway, Faridabad, Haryana, 121001, India

† Electronic supplementary information (ESI) available: Contains spectral characterization, ^{1}H-NMR, ^{13}C-NMR, HRMS spectra, and NCI *in vitro* results. See DOI: https://doi.org/10.1039/d4ra00547c

Open Access Article. Published on 22 August 2024. Downloaded on 3/8/2026 10:43:55 AM. This article is licensed under a Creative Commons Attribution-NonCommercial 3.0 Unported Licence.

anticancer activity on a panel of 60 different human cancer cell lines (at NCI).[19–23] Further, the mechanism of action for the most potent derivatives was determined against breast cancer cell line MDA-MB-231. Since the acetals of andrographolide and isoandrographolide acted as very good anticancer agents, in our present work, we intended to link the pyrazole moiety to andrographolide and isoandrographolide and investigate their potential as anticancer agents. Pyrazoles were chosen because of their significant importance as pharmacophores in forming the basis for diverse pharmaceutical compounds.[24–26]

2. Experimental

2.1. Synthesis

All the chemicals were obtained from Sigma Aldrich, HiMedia, and Alfa Aesar, while the solvents were distilled before use.

2.1.1. Synthesis of *N′*-(1-arylethylidene) isonicotinohydrazides. Isoniazid (25 mmol) was added to a solution of substituted acetophenones (25 mmol) in methanol (80 mL) and stirred at room temperature. 2 mL of glacial acetic acid was then added, and the mixture was refluxed for 8 hours. The progress of the reaction was monitored by TLC analysis. Crushed ice was added once the reaction was complete, and the resultant solid was filtered and dried. The product obtained was then recrystallized with ethanol.

2.1.2. Synthesis of 3-aryl-1-*H*-pyrazole-4-carboxaldehydes (A–I). Aliquot amounts of *N′*-(1-arylethylidene) isonicotinohydrazides (20 mmol) were added to the Vilsmeier-Haack reagent prepared from *N*,*N*-dimethylformide (20 mL) and $POCl_3$ (60 mmol) at 0 °C. The reaction mixture was stirred and heated at 65 °C for 4 hours after the addition. After the reaction was completed, the resultant mixture was poured into crushed ice. The solution was then neutralized with saturated Na_2CO_3 to obtain a solid. The product was purified by column chromatography using hexane and ethyl acetate in a 65 : 35 ratio as eluent.

2.1.3. Synthesis of 3,19-(NH-3-aryl-pyrazole) acetals of andrographolide (1a–1h). Andrographolide (1 mmol) and 3-aryl-1*H*-pyrazole-4-carbaldehydes (4 mmol) were dissolved in DMSO (3 mL) at room temperature. To this, pyridinium *para*-toluene sulfonate (PPTS) was added in a catalytic amount (0.08 mmol) and the mixture was heated at 70 °C for 24 hours. After completion of the reaction, the mixture was cooled down to room temperature and neutralized with freshly prepared cold saturated sodium bicarbonate solution. The resulting solution was then extracted three times (15 mL each) with DCM and the obtained organic layer was thoroughly washed with brine solution and dried over anhydrous sodium sulfate. DCM was removed using a rota evaporator. The crude product obtained was then purified using column chromatography (hexane : acetone, 60 : 40).

2.1.4. Synthesis of 3,19-(NH-3-aryl-pyrazole) acetals of isoandrographolide (2a–2g, 2i). First, isoandrographolide was synthesized by dissolving 8 g of andrographolide in 150 mL of conc. HCl and stirred the mixture for 24 hours at room temperature. After completion of the reaction, crushed ice was added and extracted three times with DCM (25 mL each). The organic layer was thoroughly washed with freshly prepared cold saturated sodium bicarbonate and brine solutions, dried over anhydrous Na_2SO_4, and recrystallized from ethyl acetate to get pure isoandrographolide. Then isoandrographolide was taken as starting material along with 3-phenyl-1*H*-pyrazole-4-carbaldehydes and followed the same procedure as above to synthesize the compounds **2a–2g**, **2i**.

2.2. Instrumentation

The ^{1}H and ^{13}C-NMR spectra were recorded on BRUKER ASCEND 400 MHz and 100 MHz respectively. Tetramethylsilane (TMS) was used as an internal standard. Mass spectra were generated using AGILENT 6550 Q-TOF LC-MS (HRMS). Acetonitrile was used as a solvent to record UV-vis spectra in the range 200–600 nm using a Shimadzu 2450 spectrophotometer. Using KBr pellets, FT-IR spectra were acquired in the range 400 and 4000 cm^{-1} on AGILENT Cary 630 spectrophotometer. Agilent 1260 Infinity high-performance liquid chromatography system, equipped with a quaternary solvent delivery system, inline degasser, auto sampler, and photodiode array detector, was used. Samples were examined using water (10%) and acetonitrile (90%) as mobile phase on a Zorbax Extend-C18 (4.6 mm 250 mm, 5 μm) column at a flow rate of 1 mL min^{-1}. At 25 °C, the separation was performed with an injection volume of 15 μL. A diode array detector was utilized to capture the chromatogram between 200 and 700 nm.

2.3. *In silico* studies

All the active compounds were screened for their *in silico* Lipinski and ADMET properties using the pkCSM tool.[27]

3. Biological testing

3.1. Anticancer studies

3.1.1. NCI protocol. National Cancer Institute (NCI), Bethesda, Maryland, USA, screened all the sixteen compounds for their anticancer activity against nine different cancer types, consisting of a panel of 60 human cancer cell lines. The assessment of growth inhibition percentage compared to untreated control samples was conducted using spectrophotometry. A continuous 48 h exposure approach was employed, and cell viability was determined using a sulforhodamine B protein assay. A comprehensive protocol has been provided in the ESI.†

3.1.2. Cell culture. Cancer cells (HCT-116) and Vero E6 cells were cultured in Dulbecco's modified Eagle's medium supplemented with 10% fetal bovine serum (FBS) and 1× penicillin-streptomycin solution at 37 °C and 5% CO_2. Cells were grown to 70 to 80% confluency and harvested using 1X trypsin.

3.1.3. Cell viability assay. Cancer cells (HCT-116) and Vero E6 cells (5×10^3 cells per well) were seeded in 96-well plates. Following a 24 hour incubation period, the cells were exposed to various concentrations (ranging from 100 to 0.097 μM) of test samples for 48 h. Subsequently, MTT (3-(4,5-dimethylthiazol-2-yl)-2,5-diphenyltetrazolium bromide) (10 μL) was introduced into each well and allowed to incubate for an additional 3 h.

 © 2024 The Author(s). Published by the Royal Society of Chemistry

Open Access Article. Published on 22 August 2024. Downloaded on 3/8/2026 10:43:55 AM.
This article is licensed under a Creative Commons Attribution-NonCommercial 3.0 Unported Licence.

After the incubation, the media was removed and the crystals were dissolved in 100 μL DMSO. Then, the absorbance of the plate was taken at 570 nm using a spectrophotometer. The values were plotted (% cell viability *vs.* concentration) to obtain the IC_{50} as per the previous protocol.[28]

3.1.4. Cell cycle assay. Cancer cells (HCT-116) (3×10^5 cells per well) were seeded on a 6-well plate. After a 24 h incubation, the medium was replaced with an incomplete medium lacking FBS to synchronize the cells. After 8 h synchronization period, the incomplete medium was removed, and cells were exposed to the test samples (5 μM and 10 μM) for 24 h. Subsequently, the cells were harvested using 1X trypsin, washed twice with cold 1X PBS, and fixed in 70% ethanol at 4 °C overnight. After two additional washes with PBS, the cells were treated with a staining buffer containing ribonuclease A (100 μg mL^{-1}) and propidium iodide (50 μg mL^{-1}) in 1× PBS overnight. Finally, the cells were analyzed using a flow cytometer (FACSVerse, BD Biosciences, NJ, USA).[28]

3.1.5. PI uptake assay. Cancer cells (HCT-116) (1×10^5 cells per well) were seeded in a 12-well plate. Following a 24 hour incubation period, cells were treated with the test samples (10 μM) for 48 h. Subsequently, cell harvesting was conducted using 1X trypsin, followed by a washing step with a 1X PBS solution. Staining with propidium iodide (PI) (100 μg mL^{-1}) was performed, and the stained cells were promptly acquired and analyzed using a flow cytometer (FACSVerse, BD Biosciences, NJ, USA).[28]

3.1.6. Apoptotic assay. Cancer cells (HCT-116) (3×10^5 cells per well) were seeded in a 12-well plate. After 24 h incubation, cells were treated with test samples (10 μM), and further

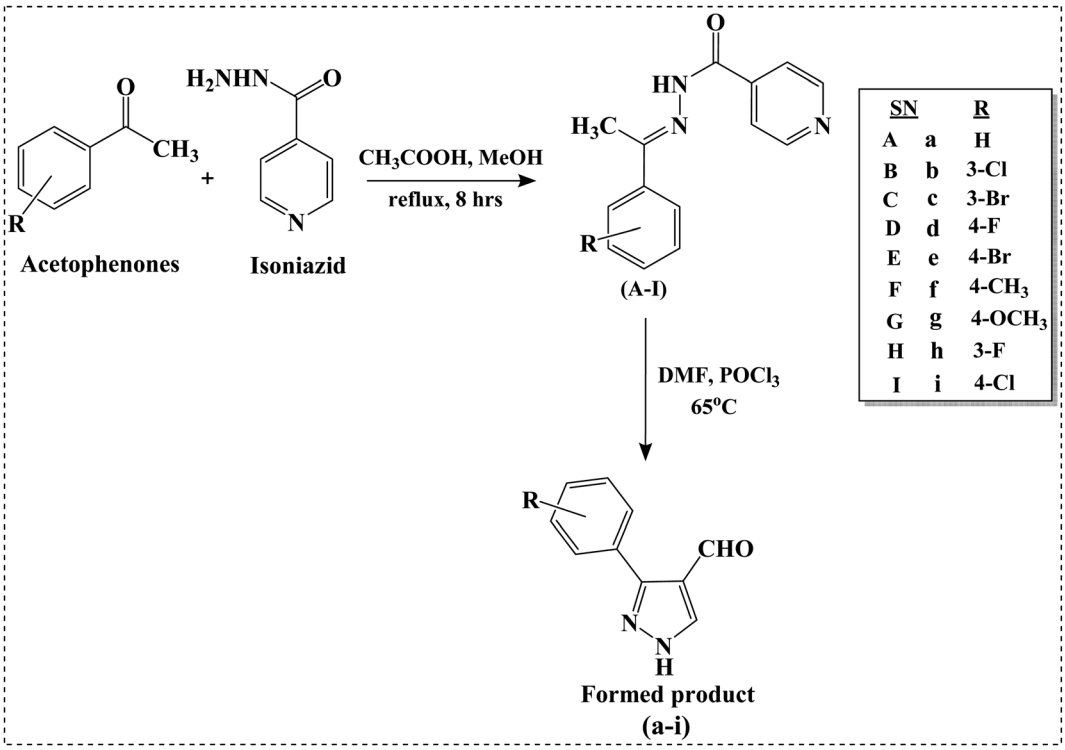

Scheme 1 Synthesis of *N′*-(1-arylethylidene) isonicotinohydrazides (**A–I**) and 3-aryl-1*H*-pyrazole-4-carbaldehydes (**a–i**).

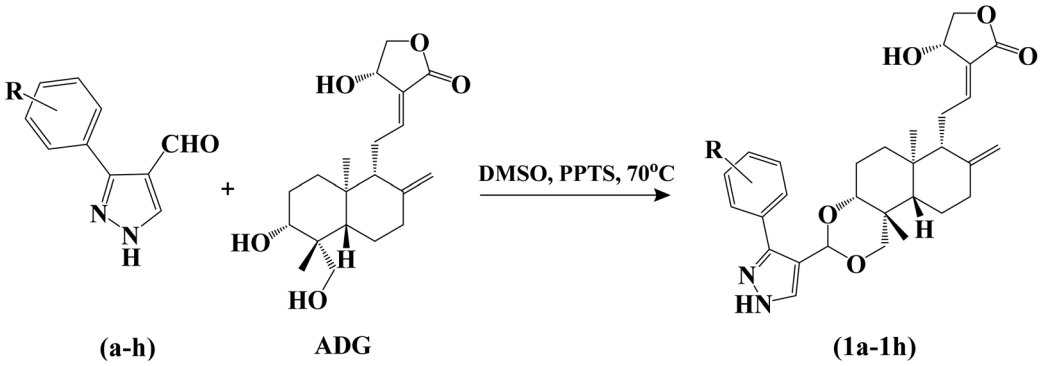

Scheme 2 Synthesis of 3,19-(NH-3-aryl-pyrazole) acetals of andrographolide (**1a–1h**).

Open Access Article. Published on 22 August 2024. Downloaded on 3/8/2026 10:43:55 AM.
This article is licensed under a Creative Commons Attribution-NonCommercial 3.0 Unported Licence.

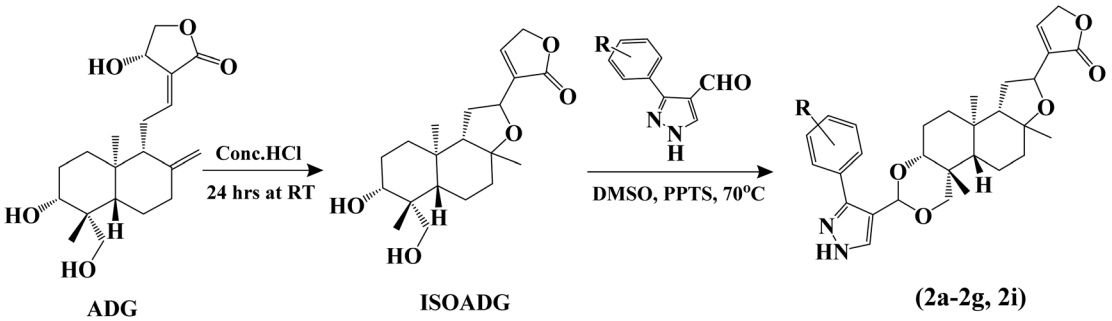

Scheme 3 Synthesis of isoandrographolide and 3,19-(NH-3-aryl-pyrazole) acetals of isoandrographolide (**2a–2g** and **2i**).

incubated for 48 h. The supernatant (for dead cells) and adherent cells were both collected by introducing 1X trypsin for 5 min, followed by centrifugation at 4000 rpm for 5 min. The collected cells were then resuspended in 100 μL of 1X annexin V binding buffer. Annexin V–FITC staining (1 μL) was added to the cells, which were then vortexed and left in the dark at 4 °C for 15 min. Subsequently, propidium iodide solution (100 μg mL^{-1}) was added to each vial, incubated for 15 min, and cells were promptly analyzed using a flow cytometer (FACSVerse, BD Biosciences, NJ, USA).[28]

3.1.7. ROS assay. Cancer cells (HCT-116) (1×10^5 cells per well) were plated in a 12-well plate. Following 24 h incubation period, cells underwent a wash with 1X PBS and were exposed to 2.5 μL (10 mM) DCHF-DA (2,7-dichlorodihydrofluorescein diacetate) for 30 min in 0.2% FBS in DPBS. Subsequent to this incubation, another wash with 1× PBS was performed to eliminate excess dye solution. Cells were then treated with the test sample (10 μM), and incubated for an additional 3 h. Cell harvesting was carried out using 1X trypsin, and cells were immediately analysed using a flow cytometer (FACSVerse, BD Biosciences, NJ, USA).[28]

4. Results and discussion

4.1. Chemistry

We intend to synthesize 1-isonicotinoyl-3-aryl-1*H*-pyrazole-4-carbaldehydes and further prepare their acetals with andrographolide and isoandrographolide. In step-1, we synthesized nine *N*′-(1-arylethylidene) isonicotinohydrazides (**A–I**), and in step-2, they were to be converted to 1-isonicotinoyl-3-aryl-1*H*-pyrazole-4-carbaldehydes (**a–i**) in the presence of DMF, $POCl_3$ (1.2 equivalents) at 65 °C as reported by Beniwal *et al.*[29] However, surprisingly, when we used 3 equivalents of $POCl_3$, we observed the formation of 3-aryl-1*H*-pyrazole-4-carbaldehydes (**a–i**) instead of 1-isonicotinoyl-3-aryl-1*H*-pyrazole-4-carbaldehydes (Scheme 1). To investigate the effect of $POCl_3$ in this reaction, we repeated the procedure using 2 equivalents of $POCl_3$. However, we again observed the formation of 3-aryl-1*H*-pyrazole-4-carbaldehydes (**a–i**). This is the first report of the synthesis of 3-aryl-1*H*-pyrazole-4-carbaldehydes in a two-step reaction. Four of the nine synthesized carbaldehydes are novel (**c**, **e**, **f**, and **g**) in our work. Other five of these carbaldehydes were synthesized by You *et al.*, following a three-step reaction and patented the work.[30] In step-3, 3-aryl-1*H*-pyrazole-4-carbaldehydes (**a–i**) were reacted with andrographolide (ADG) (Scheme 2) and isoandrographolide (ISOADG) (Scheme 3) in the presence of mild acid catalyst pyridinium *para*-toluene sulfonate (PPTS) to obtain the desired products (**1a–1h**, **2a–2g**, **2i**). All the products were purified using column chromatography.

4.1.1. Probable mechanism for the formation of 3-aryl-1*H*-pyrazole-4-carbaldehydes (a–i). Step-1: formation of iminium ion intermediate from DMF and $POCl_3$.

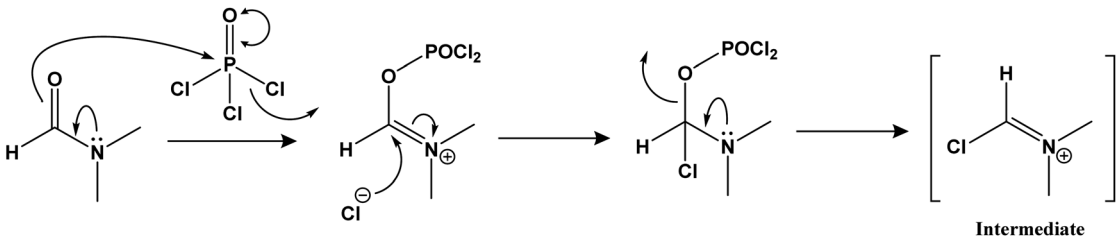

Step-2: reaction of *N*′-(1-arylethylidene) isonicotinohydrazides with iminium ion.

Step-3: nucleophile attack on the amide carbonyl to form 3-aryl-1*H*-pyrazole-4-carbaldehydes.

The amide carbonyl, as seen in step-3 above, is linked to two electron-withdrawing groups (pyridine and pyrazole-4-carboxaldehyde). This makes it more prone to react with nucleophiles. Hence, the possible mechanism for the formation of 3-aryl-1*H*-pyrazole-4-carbaldehydes (**a–i**) instead of 1-isonicotinoyl-3-aryl-1*H*-pyrazole-4-carbaldehydes could involve nucleophilic attack at the amide carbonyl, resulting in the hydrolysis of the amide bond.

4.1.2. Characterization. The UV-vis spectra exhibited bands between 230 and 250 nm for all the acetals. In the IR spectra of

 © 2024 The Author(s). Published by the Royal Society of Chemistry

Open Access Article. Published on 22 August 2024. Downloaded on 3/8/2026 10:43:55 AM.
This article is licensed under a Creative Commons Attribution-NonCommercial 3.0 Unported Licence.

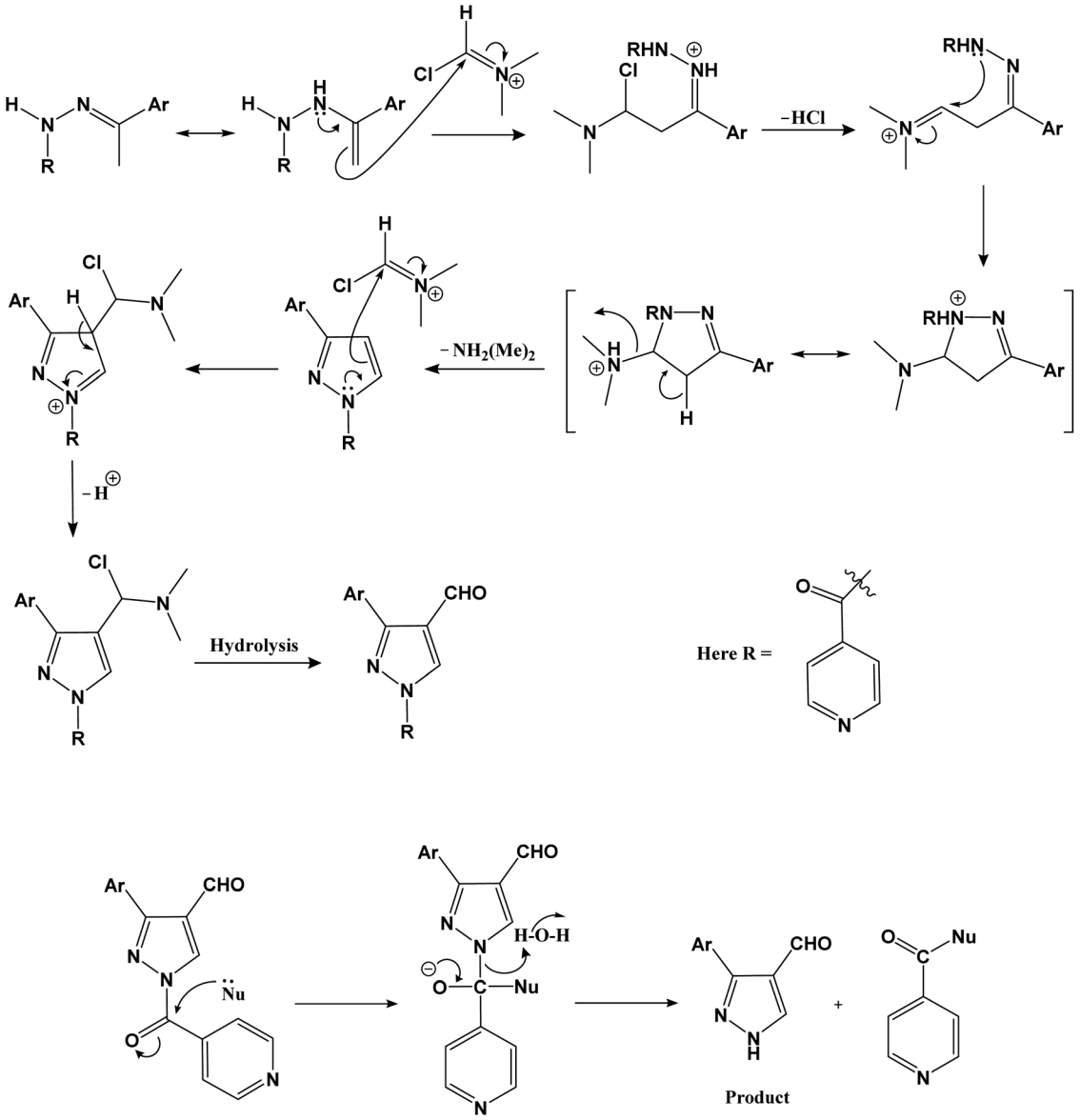

3,19-(NH-3-aryl-pyrazole) acetals of andrographolide, a peak in the range 3520–3401 cm^{-1} was observed for –OH whereas a peak at ~1675 cm^{-1} corresponds to exocyclic C=C groups. These peaks were absent for 3,19-(NH-3-aryl-pyrazole) acetals of isoandrographolide. –NH stretching peak in all the acetals appeared in the range 3321–3270 cm^{-1}. The peak at ~1755 cm^{-1} corresponds to the carbonyl group (C=O) of the lactone moiety. Distinct absorptions at approximately 1200 to 1100 cm^{-1} can be attributed to the C–O stretching bands. Compounds with aryl chloride have bands at ~1150 cm^{-1} (Ar–Cl stretch). Compounds with aryl fluorides showed a band around 1234 and 1219 cm^{-1} (Ar–F stretch), and compounds with aryl bromides have a band between 1018–1010 cm^{-1} (Ar–Br stretch).

In the ^{1}H NMR spectra of all the acetals, the signal around δ 7.80 is attributed to the presence of H-5′, while peaks within the range of δ 7.90 to 6.95 correspond to the aromatic protons linked to the pyrazole ring (H-7′ to H-11′). The proton signal for the unsaturated lactone (H-14) in 3,19-(NH-3-aryl-pyrazole) acetals of isoandrographolide is observable at ~δ 7.29. Additionally, the peak at around δ 6.95 corresponds to H-12 in 3,19-(NH-3-aryl-pyrazole) acetals of andrographolide. Across all compounds, a singlet peak at ~δ 5.82 is for H-21.

In the ^{13}C NMR spectra, signals approximately within the range of δ 173–170, confirm the presence of a carbonyl group (C=O). The carbons in the pyrazole ring, aromatic ring, and olefin carbons were identified in the ~δ 163 to 110 range. Notably, in the case of 3,19-(NH-3-aryl-pyrazole) acetals of isoandrographolide, the olefin carbons such as C-8 and C-17 are absent, leading to the absence of a signal around δ 110. A distinct signal around δ 90, associated with C-21 bonded to two oxygen atoms, strongly supports the formation of acetals. Carbon signals related to oxygen atoms (–O–C) were observed within the range of δ 82 to 66.[31,32] The complete characterization

Open Access Article. Published on 22 August 2024. Downloaded on 3/8/2026 10:43:55 AM. This article is licensed under a Creative Commons Attribution-NonCommercial 3.0 Unported Licence.

and spectral data of the compounds (**A–I**, **a–i**, **1a–1h**, **2a–2g**, and **2i**) is provided in the ESI.†

4.2. Biological evaluation

4.2.1. NCI anticancer screening. Anticancer potential of the sixteen newly synthesized 3,19-(NH-3-aryl-pyrazole) acetals of andrographolide and isoandrographolide was tested against a panel of 60 different human cancer cell lines spanning across nine human cancer types such as leukaemia, non-small lung cancer, colon, central nervous system (CNS), melanoma, ovarian, renal, prostate, and breast cancer by National Cancer Institute (NCI, USA). Initially, all sixteen compounds (**1a–1h**, **2a–2g**, and **2i**) were tested at 10 μM (one dose) on 60 cell lines. Out of which, seven compounds (**1a–1g**) satisfied pre-determined threshold inhibition criteria in a minimum number of cell lines (one dose study result of these seven compounds is given in the ESI (Table S1)).† Therefore, these seven compounds were further selected for their five dose screening to obtain GI_{50} (50% growth inhibitory activity), TGI (Total growth inhibition), and LC_{50} (50% lethal concentration) values on all the cell lines by NCI. Interestingly, all seven compounds (**1a–1g**) that are active on most of the cell lines at 10 μM were 3,19-(NH-3-aryl-pyrazole) acetals of andrographolide. However, 3,19-(NH-3-aryl-pyrazole) acetals of isoandrographolide have exhibited less % growth inhibition indicating that these derivatives are less active on the majority of the cell lines due to which they were not selected for five dose studies.

4.2.2. Five dose study. Five dose screening results revealed that four out of seven compounds: *meta*-substituted –Br and –Cl derivatives (**1c** and **1b**) and *para*-substituted –Br and $-OCH_3$ derivatives (**1e** and **1g**) are highly active and displayed excellent GI_{50}s against majority of the cell lines (Table 1). Among the four compounds, compound **1c** was observed to be the most potent, followed by compound **1b** against almost all the cell lines.

Both *meta* and *para* substituted –Br derivatives **1c** and **1e** showed the highest activity with GI_{50}s 1.28 μM and 2.13 μM respectively, against breast cancer cells MCF7, and compounds **1b** and **1g** demonstrated better activity on the MDA-MB-468 cell line with GI_{50}s 1.88 μM and 2.17 μM.

All four compounds showed promising activity on four different leukemia cancer cell lines HL-60(TB) (**1c**, GI_{50}: 1.87 μM), RPMI-8226 (**1b**, GI_{50}: 2.25 μM), K-562 (**1e**, GI_{50}: 2.24 μM) and CCRF-CEM (**1g**, GI_{50}: 2.08 μM). Compounds **1c** (GI_{50}: 1.66 and 1.75 μM) and **1b** (GI_{50}: 1.79 and 1.93 μM) have exhibited potent activity against the colon and ovarian cancer cell lines HCT-15 and NCI/ADR-RES, respectively. However, compounds **1e** and **1g** showed their superior activity on HCT-116 (GI_{50}: 1.93 and 1.86 μM) and OVCAR-3 (GI_{50}: 2.08 and 2.26 μM) cell lines.

The compounds **1c**, **1b**, and **1e** have the best activity on the melanoma cancer cell line LOX IMV (GI_{50}s: 1.39, 1.44 and 1.37 μM respectively), the renal cancer cell line RXF 393 (GI_{50}s: 1.81, 1.66 and 1.93 μM), non-small lung cancer cell line NCI-H226 (GI_{50s}: 1.62, 1.73 and 1.90 μM) and the CNS cancer cell line SF-539 (GI_{50}s: 1.74, 1.77 and 2.20 μM). In contrast, compound **1g** displayed better activity against SK-MEL-5 (GI_{50}: 1.52 μM), UO-31 (GI_{50}: 1.70 μM), NCI-H460 (GI_{50}: 1.91 μM) and SNB-75 (GI_{50}: 1.75 μM) cell lines. All four compounds were more active on the prostate cancer cell line PC-3 with GI_{50}s 3.07 μM (**1c**), 4.08 μM (**1b**), 2.13 μM (**1e**) and 2.98 μM (**1g**).

Total growth inhibition (TGI) and 50% lethal concentration (LC_{50}) of these four compounds against the 60 human cancer cell lines are provided in the ESI (Tables S2 and S3).†

4.2.3. Effect of 3,19-(NH-3-aryl-pyrazole) acetals of andrographolide on proliferation of colon cancer HCT-116 cell line. Out of the above four compounds (**1b**, **1c**, **1g**, and **1e**), three compounds (**1b**, **1c**, and **1g**) that have demonstrated excellent anticancer properties in the five dose study on the 60-cell line panel at NCI were selected for further cytotoxicity studies on the colon cancer cell line HCT-116. As shown in Table 2, the compound **1g** significantly inhibited cell proliferation of HCT-116 cells with an IC_{50} of 3.08 μM followed by **1c** (3.16 μM) and **1b** (3.40 μM). Since the compound **1g** exhibited a better IC_{50} than the other compounds, it was further selected to test against Vero E6 cells (the immortalized cell line established from kidney epithelial cells of the African green monkey). Compound **1g** was found to be non-toxic to Vero E6 cells till 20 μM concentration, and its cytotoxic concentration CC_{50} was 47.97 μM.

4.2.4. Cell cycle analysis of 1g. As compound **1g** exhibited the best IC_{50} value against the HCT-116 cell line and a low inhibitory effect on Vero E6 cells, we sought to investigate whether its inhibition was linked to its interference with the cell cycle. To identify this, HCT-116 cells were subjected to dose-dependent treatments with **1g** at concentrations of 5 μM and 10 μM. Remarkably, our observations, as depicted in Fig. 1a–d, indicate that compound **1g** induced cell accumulation in the G0/G1 phase at both 5 μM and 10 μM concentrations. This effect showed a concentration-dependent increase in the percentage of cells in the G0/G1 phase compared to the control (untreated cells, Fig. 1a). At a concentration of 5 μM (Fig. 1b and d), **1g** was responsible for the accumulation of HCT-116 cells in the G0/G1 phase, leading to a reduced percentage of cells in the S and G2/M phases. At a concentration of 10 μM (Fig. 1c and d), it was observed that a slightly higher percentage of cells were arrested in the G0/G1 as compared to the cells treated with **1g** at 5 μM concentration. Arresting cell cycle progression in G0/G1 phase indicates cells undergo repair mechanisms or follow the apoptotic pathway. To determine this, propidium iodide uptake, annexin V-FITC/PI, and reactive oxygen species assays (ROS) were performed.

4.2.5. Annexin V-FITC/PI assay. The extent of apoptosis triggered by compound **1g** in HCT-116 cells was investigated using annexin V/propidium iodide dual staining that enables the identification of different cell states like live cells, early apoptotic cells, late apoptotic cells, and necrotic cells.[33] It was observed that compound **1g** causes a noticeable increase in the percentage of early apoptotic cells (Fig. 2a–c). These findings provide evidence that compound-induced apoptosis is responsible for inhibiting HCT-116 cell proliferation.

4.2.6. ROS assay. Maintaining a stable redox environment is crucial for various cellular functions. Cancer cells exhibit elevated levels of reactive oxygen species (ROS) compared to healthy cells. However, cancer cells manage to uphold their

 © 2024 The Author(s). Published by the Royal Society of Chemistry

Open Access Article. Published on 22 August 2024. Downloaded on 3/8/2026 10:43:55 AM.
This article is licensed under a Creative Commons Attribution-NonCommercial 3.0 Unported Licence.

Table 1 Growth inhibition (50%) of the potent compounds against the NCI human cancer cell line panel

		GI_{50} (μM)			
Cancer	Sub panel	**1c** (R = 3-Br)	**1b** (R = 3-Cl)	**1g** (R = 4-OCH_3)	**1e** (R = 4-Br)
Leukemia	CCRF-CEM	NT[a]	2.70	**2.08**	2.81
	HL-60(TB)	**1.87**	2.91	2.69	2.30
	K-562	1.93	2.41	2.71	**2.24**
	MOLT-4	2.29	3.83	2.21	2.86
	RPMI-8226	2.14	**2.25**	2.60	2.56
	SR	NT	NT	2.87	NT
Non-small cell lung	A549/ATCC	3.37	9.73	3.32	11.10
	EKVX	2.15	3.68	2.66	4.69
	HOP-62	3.78	15.30	3.44	18.90
	HOP-92	2.21	4.29	2.02	5.08
	NCI-H226	**1.62**	**1.66**	3.58	**1.93**
	NCI-H23	1.84	4.36	2.51	10.50
	NCI-H322M	5.09	10.40	4.71	12.50
	NCI-H460	2.43	8.87	**1.91**	12.60
	NCI-H522	1.90	1.75	2.49	2.08
Colon	COLO 205	2.18	4.85	1.95	4.45
	HCC-2998	1.87	3.49	2.87	9.11
	HCT-116	1.83	1.84	**1.86**	**1.94**
	HCT-15	**1.66**	**1.79**	2.53	1.97
	HT29	2.10	2.70	2.86	2.80
	KM12	2.44	3.29	2.38	7.17
	SW-620	2.22	2.35	2.29	2.33
CNS	SF-268	12.60	17.30	3.25	16.50
	SF-295	1.83	4.27	2.13	12.10
	SF-539	**1.74**	**1.77**	2.03	**2.20**
	SNB-19	2.45	2.41	**1.75**	7.04
	SNB-75	NT	NT	4.42	NT
	U251	1.81	2.15	2.77	6.83
Melanoma	LOX IMVI	**1.39**	**1.44**	1.73	**1.37**
	MALME-3M	1.93	1.84	1.74	3.98
	M14	2.52	2.19	3.14	3.40
	MDA-MB-435	3.40	2.47	2.24	3.24
	SK-MEL-2	2.55	2.71	3.97	5.85
	SK-MEL-28	1.93	1.98	2.54	2.13
	SK-MEL-5	1.75	2.27	**1.52**	1.04
	UACC-257	2.85	11.20	2.46	11.8
	UACC-62	1.55	1.69	1.68	3.44
Ovarian	IGROV1	2.72	4.15	3.98	13.80
	OVCAR-3	2.02	1.93	**2.26**	**2.08**
	OVCAR-4	4.47	4.40	2.96	5.02
	OVCAR-5	2.14	3.64	3.90	10.00
	OVCAR-8	1.88	2.39	3.34	3.24
	NCI/ADR-RES	**1.75**	**1.93**	NT	2.20
	SK-OV-3	5.80	16.00	10.50	16.80
Renal	786–0	1.92	3.36	1.92	5.75
	A498	2.08	1.85	17.00	16.80
	ACHN	**1.95**	2.47	3.52	2.16
	CAKI-1	2.77	4.00	2.96	8.18
	RXF 393	1.81	**1.73**	1.74	**1.90**
	SN12C	2.03	2.94	3.54	7.51
	TK-10	5.10	12.40	4.12	18.40
	UO-31	NT	NT	**1.70**	NT
Prostate	PC-3	**3.07**	**4.08**	**2.98**	**4.08**
	DU-145	3.08	5.01	3.23	8.24
Breast	MCF7	**1.28**	2.06	2.48	**2.13**
	MDA-MB-231/ATCC	NT	NT	2.39	NT
	HS 578T	5.27	9.04	2.20	17.70
	BT-549	1.44	2.36	2.36	2.88
	T-47D	NT	NT	3.25	NT
	MDA-MB-468	1.61	**1.88**	**2.17**	2.47

[a] NT – not tested.

Open Access Article. Published on 22 August 2024. Downloaded on 3/8/2026 10:43:55 AM.
This article is licensed under a Creative Commons Attribution-NonCommercial 3.0 Unported Licence.

Table 2 IC_{50} values of the potent compounds **1b**, **1c**, and **1g** against the HCT-116 cell line

Compound	IC_{50} (μM)
1g	3.08
1c	3.16
1b	3.40

redox equilibrium due to their robust antioxidant defenses. Nevertheless, the heightened accumulation of ROS can perturb redox homeostasis and result in substantial damage to cancer cells.[34] Since we noticed that compound **1g** was associated with cell apoptosis, we were interested in investigating whether this effect was linked to the generation of ROS in HCT-116 cells. Interestingly, following the exposure of HCT-116 cells to **1g** (10 μM), there was a significant rise in intracellular ROS levels when compared to the control (Fig. 3). These findings suggest that the apoptosis of HCT-116 cells induced by compound **1g** can be mainly attributed to the elevated levels of ROS.

4.3. Structural activity relationship based on NCI screening

As mentioned before, our group previously investigated the anticancer properties of 3,19-benzylidene/heteroaromatic

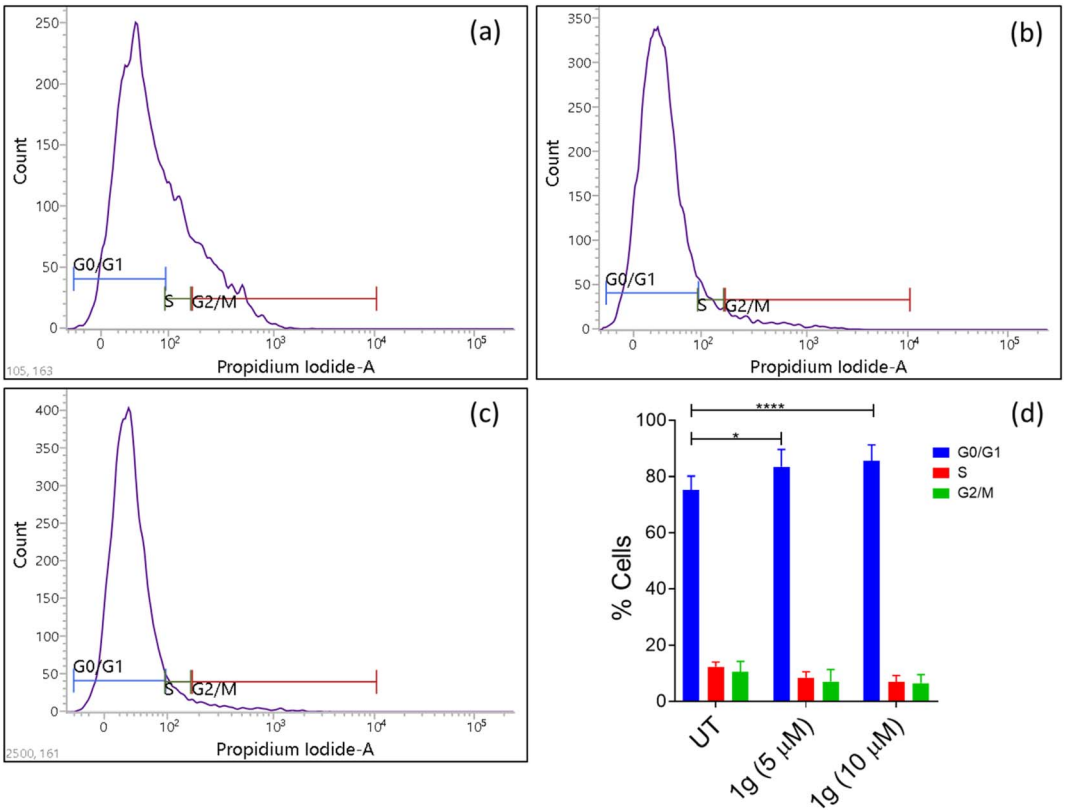

Fig. 1 Effect of compound **1g** on HCT-116 cell cycle arrest. (a) Untreated (control); (b) HCT-116 cells treated with 5 μM concentration of **1g**; (c) HCT-116 cells treated with 10 μM concentration of **1g**; (d) % cells in each phase after treatment with **1g**.

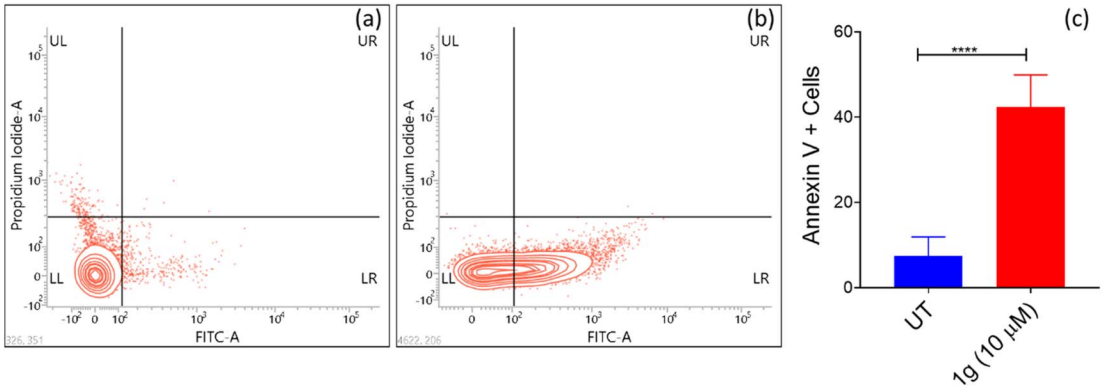

Fig. 2 Flow cytometry plots using Annexin V-FITC/PI staining for apoptosis. HCT-116 cells were treated with (a) control (untreated cells) (b) 10 μM concentration of **1g**. (c) % of apoptotic cells after treatment with **1g**.

 © 2024 The Author(s). Published by the Royal Society of Chemistry

Open Access Article. Published on 22 August 2024. Downloaded on 3/8/2026 10:43:55 AM.
This article is licensed under a Creative Commons Attribution-NonCommercial 3.0 Unported Licence.

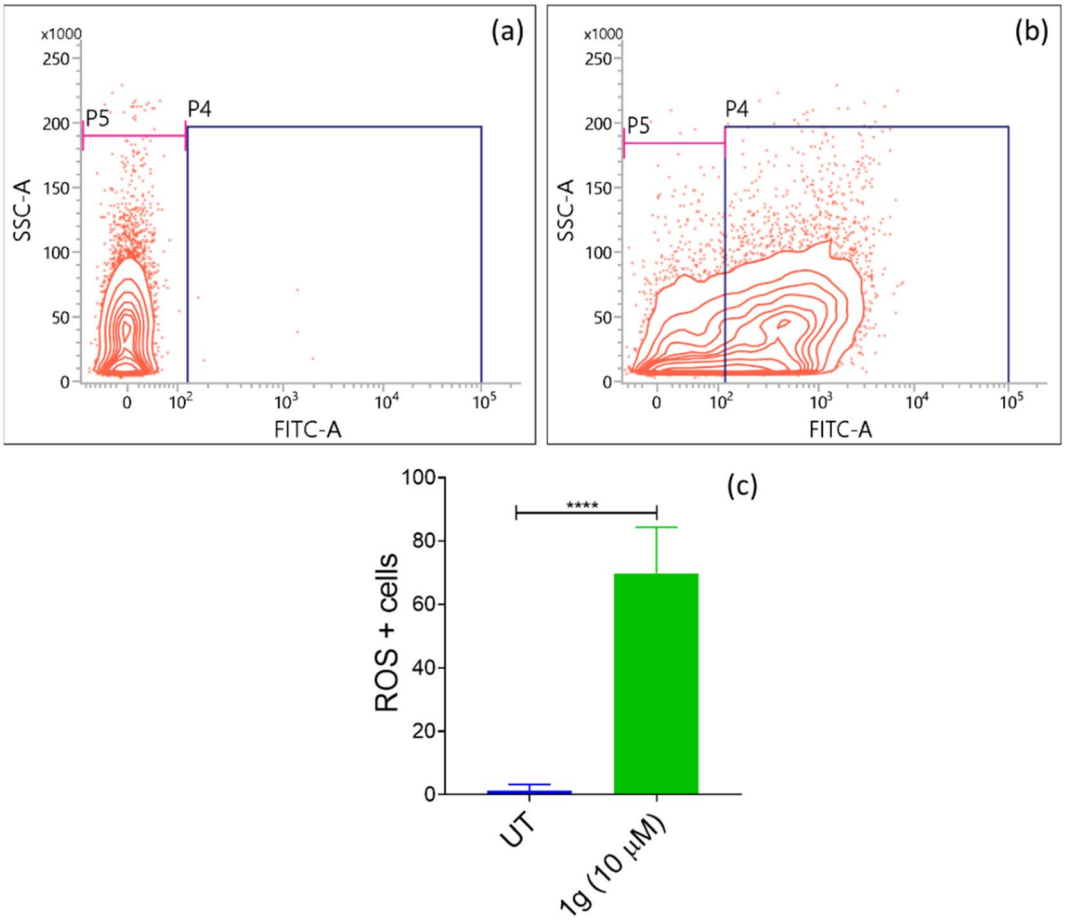

Fig. 3 Determination of intracellular ROS levels in HCT-116 cells treated with (a) control (untreated cells), (b) 10 μM concentration of **1g**; (c) % of ROS levels in the presence of **1g**.

Table 3 Comparison of % growth inhibition of benzylidene/heteroaromatic/pyrazole acetals of andrographolide on a human cancer cell line panel

		% Growth inhibition							
Cancer	Cell line	ADG	Bz-ADG	Fur-ADG	Py-ADG	Thio-ADG	**1c**	**1b**	**1g**
Leukaemia	CCRF-CEM	76.51	90.97	89.84	86.21	66.78	−15.57	−14.87	99.40
	HL-60(TB)	n.a[a]	51.12	1.86	13.79	n.a	−16.26	−15.08	98.41
	K-562	34.47	56.31	55.44	47.29	23.54	−2.18	95.00	−31.21
	RPMI-8226	16.71	71.77	82.88	58.08	29.46	−6.49	−11.69	−27.00
	SR	20.46	63.12	70.99	83.82	23.59	97.32	84.29	−29.91
NSCL	NCI-H522	82.86	36.48	36.90	34.87	15.89	−55.96	−59.98	−18.40
Colon	HCT-116	39.98	61.62	48.53	38.35	15.56	−95.92	−91.58	−19.04
	HCT-15	38.11	34.48	40.82	28.68	13.59	−67.53	−59.20	−35.29
	HT29	72.99	45.20	36.91	30.12	15.95	98.48	99.69	−26.28
	SW-620	55.71	50.33	54.62	51.49	8.40	−81.14	−57.57	n.t
Melanoma	LOX IMVI	78.16	66.18	77.96	77.02	27.00	−100	−100	n.t
Ovarian	OVCAR-8	15.52	43.42	42.62	26.37	21.32	−42.49	−23.31	−3.29
	NCI/ADR-RES	16.25	42.98	23.28	12.07	6.23	−50.15	−56.43	93.33
Breast	MCF7	42.44	53.91	51.30	36.01	27.86	−48.20	−52.32	98.00
	BT-549	12.88	36.15	n.a	n.a	n.a	−94.24	−92.39	−32.90

[a] n.a – not active; n.t – not tested, negative values represent lethality (example: −15.57% growth inhibition means 15.57% lethality).

Open Access Article. Published on 22 August 2024. Downloaded on 3/8/2026 10:43:55 AM.
This article is licensed under a Creative Commons Attribution-NonCommercial 3.0 Unported Licence.

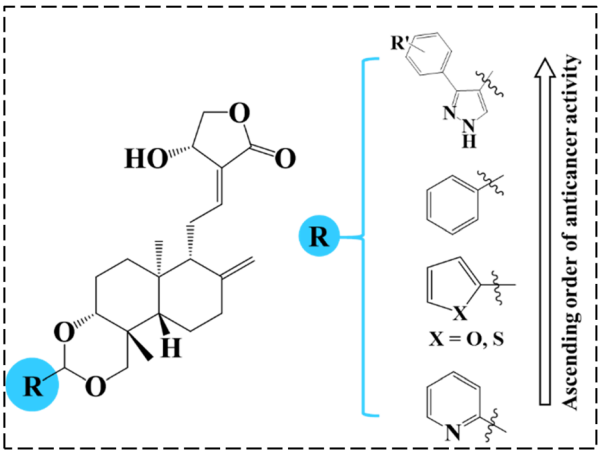

Fig. 4 The order of anticancer activity of benzylidene/heteroaromatic/pyrazole acetals of andrographolide.

Table 4 Lipinski parameters of the active compounds

Compounds	Lipinski parameters				
	MW[a]	MR	#H.D	#H.A	Log *P*
1b	538	93.67	2	7	4.76
1c	582	93.67	2	7	4.93
1g	534	102.90	2	8	4.07

[a] MW – molecular weight, MR – molar refractivity, #H.D – no. of. hydrogen bonds, #H.A – no. of. hydrogen bond acceptors. Log *P* – partition coefficient.

acetals of andrographolide and isoandrographolide.[22] These derivatives have displayed moderate to good anticancer activity. Therefore, from these series, we have selected and compared the most active compounds and the cell lines on which they showed good activity with the top three 3,19-(NH-3-aryl-pyrazole) acetals of andrographolide (**1c**, **1b** and **1g**) (% growth inhibition -Table 3, Fig. 4). Interestingly, on all the cell lines, the compounds **1c**, **1b** and **1g** exhibited several-fold better % growth inhibition than the rest of the compounds. Indeed, these three compounds are lethal to most of the cancer cell lines. Here, the better anticancer activity could be attributed to the presence of pyrazole moiety in the acetals of andrographolide or isoandrographolide.

4.4. Drug-likeness and ADMET prediction

Employing the pkCSM tool, *in silico* drug-likeness, pharmacokinetic, and toxicity studies (Table 4 and 5) were performed for the active compounds in order to determine their potential as drug candidates by analysing their Lipinski and ADMET parameters.

From the results, we note that the *in silico* molecular properties of the active compounds are in accordance with Lipinski's rule of five (RO5) barring molecular weights. The molecular weights of all the active compounds are in the range of 534–582 Daltons, slightly exceeding the acceptable limit (<500 Dalton). However, molecular weights of natural products are frequently considered an exception to Lipinski's rules.[35] Molar refractivity of the compounds was found to be in the range 40–130 and Log *P* was observed to be <5. The total number of *N*–H and O–H hydrogen bond donors is <5 and the number of nitrogen and oxygen-hydrogen bond acceptors (HBA) is <10.

Table 5 ADMET properties of the active compounds

ADMET	Compound		
	1b	**1c**	**1g**
Water solubility (Log *s*)	−5.24	−5.27	−5.01
Skin permeability (Log K_p)	−2.84	−2.83	−2.83
GI absorption	High	High	High
BBB permeability	Low	Low	Low
CYP1A2 inhibitor	No	No	No
Total clearance	0.17	0.15	0.18
Max. tolerated dose	−0.860	−0.862	−0.845
AMES toxicity	No	No	No
hERG inhibitor	No	No	No
Skin sensitization	No	No	No
Minnow toxicity	−1.419	−1.56	−1.56

We also examined the adsorption, distribution, metabolism, excretion, and toxicity effects of the active compounds using pkCSM to obtain a comprehensive picture of their therapeutic efficacy.

Table 5 provides an overview of the ADMET properties of the various compounds with potential for use as drugs. The compounds showed moderate aqueous solubility, high gastrointestinal absorption, and low BBB permeability. In addition, log K_p and maximum tolerated dose values were observed to be in the acceptable range, and all the compounds are non-inhibitors of CYP1A2 and hERG. Importantly, none of the compounds exhibited AMES toxicity, hERG inhibition, skin sensitization, and minnow toxicity. Compliance with Lipinski's parameters and the observed ADMET properties indicate that these molecules deserve to be investigated as potential anticancer agents.

5. Conclusion

In conclusion, nine 3-aryl-1*H*-pyrazole-4-carbaldehydes were synthesized, and among these four are novel. These pyrazole carbaldehydes were used as starting materials to synthesize eight 3,19-(NH-3-aryl-pyrazole) acetals of andrographolide and eight 3,19-(NH-3-aryl-pyrazole) acetals of isoandrographolide. All the synthesized compounds (**1a–1h**, **2a–2g**, **2i**) have been characterized extensively and were initially tested at the NCI (USA) for their anticancer properties on a panel of 60 human cancer cell lines. Interestingly, 3,19-(NH-3-aryl-pyrazole) acetals of andrographolide exhibited better anticancer activity than the acetals of isoandrographolide. Seven out of the eight 3,19-(NH-3-aryl-pyrazole) acetals of andrographolide (**1a–1g**) were further selected for five dose study to determine GI_{50}s, total growth inhibition, and LC_{50}s by NCI. The most potent among them (**1b**,

 © 2024 The Author(s). Published by the Royal Society of Chemistry

Open Access Article. Published on 22 August 2024. Downloaded on 3/8/2026 10:43:55 AM. This article is licensed under a Creative Commons Attribution-NonCommercial 3.0 Unported Licence.

1c, and **1g**) were further chosen to find out their IC_{50}s against the colon cancer HCT-116 cell line. Based on the IC_{50} values, the most potent compound **1g** (IC_{50} 3.08 μM) was selected to investigate its mechanism of action on the HCT-116 cell line. The results revealed that **1g** was responsible for the cell cycle arrest at the G0/G1 phase due to the early apoptosis of HCT-116 cells. In addition, ROS assay results indicated that the apoptosis of HCT-116 cells induced by compound **1g** was mainly attributed to the elevated levels of intracellular ROS in HCT-116 cells. Further, the best three active compounds (**1c**, **1b** and, **1g**) were found to be more active than 3,19-benzylidene/heteroaromatic acetals of andrographolide and isoandrographolide, which were previously synthesized by our group. This comparison indicates that the pyrazole moiety played a crucial role in improving the anticancer activity. Further, *in silico* Lipinski and ADMET results of the most active compounds suggest that these can be modeled as potential therapeutic leads for the treatment of cancer.

Data availability

The data supporting this article have been included as part of the ESI.†

Author contributions

Siva Kumar Rokkam carried out the synthesis, characterization, *in silico* studies, data analysis, and drafted the manuscript. Manohar Bhujel and Dolly Jain performed and analysed the *in vitro* anticancer studies: cell viability, cytotoxicity, cell cycle analysis, staining, and ROS assays. Avinash Bajaj supervised the anticancer studies. Nageswara Rao Golakoti, Lakshminath Sripada and Srinivas Nanduri conceived the study, participated in its design, analyzed the results, and contributed to drafting the manuscript. All authors read and approved the final manuscript.

Conflicts of interest

There are no conflicts to declare.

Acknowledgements

The authors dedicate this work to the Founder Chancellor Bhagawan Sri Sathya Sai Baba. We thank the Central Research Instruments Facility-SSSIHL for providing the characterization facilities. Authors thank the Disease Biology lab, SSSIHL and Regional Center for Biotechnology (RCB) for providing lab facilities to carry out biological studies. GNR and NS are grateful to the Council of Scientific & Industrial Research (CSIR) for funding this project (no. 02(0304)/17/EMR-II).

References

1 C. Aromdee, *Expert Opin. Ther. Pat.*, 2012, **22**, 169–180.
2 S. G. S. Kandanur, N. Tamang, N. R. Golakoti and S. Nanduri, *Eur. J. Med. Chem.*, 2019, **176**, 513–533.
3 M. Jiang, F. Sheng, Z. Zhang, X. Ma, T. Gao, C. Fu and P. Li, *J. Ethnopharmacol.*, 2021, **272**, 113954.
4 P. Sharma, N. Kumar and R. Dudhe, *Pharmacologyonline*, 2011, **2**, 11.
5 S. Kumar, B. Singh and V. Bajpai, *J. Ethnopharmacol.*, 2021, **275**, 114054.
6 A. Okhuarobo, J. Ehizogie Falodun, O. Erharuyi, V. Imieje, A. Falodun and P. Langer, *Asian Pac. J. Trop. Dis.*, 2014, **4**, 213–222.
7 L. S. Chua, *Phyther. Res.*, 2014, **28**, 1589–1598.
8 A. Widyawaruyanti, M. Asrory, W. Ekasari, D. Setiawan, A. Radjaram, L. Tumewu and A. F. Hafid, *Procedia Chem.*, 2014, **13**, 101–104.
9 A. K. Jadhav and S. M. Karuppayil, *Phyther. Res.*, 2021, **35**, 5365–5373.
10 R. A. Kumar, K. Sridevi, N. V. Kumar, S. Nanduri and S. Rajagopal, *J. Ethnopharmacol.*, 2004, **92**, 291–295.
11 Y. Dai, S.-R. Chen, L. Chai, J. Zhao, Y. Wang and Y. Wang, *Crit. Rev. Food Sci. Nutr.*, 2019, **59**, S17–S29.
12 J. C. W. Lim, T. K. Chan, D. S. W. Ng, S. R. Sagineedu, J. Stanslas and W. S. F. Wong, *Clin. Exp. Pharmacol. Physiol.*, 2012, **39**, 300–310.
13 G. Liu and H. Chu, *Oncol. Lett.*, 2018, **15**, 5301–5305.
14 P. Udomwan, C. Pientong, P. Tongchai, A. Burassakarn, N. Sunthamala, S. Roytrakul, S. Suebsasana and T. Ekalaksananan, *Int. J. Mol. Sci.*, 2021, **22**, 6806.
15 Z. Malik, R. Parveen, B. Parveen, S. Zahiruddin, M. Aasif Khan, A. Khan, S. Massey, S. Ahmad and S. A. Husain, *J. Ethnopharmacol.*, 2021, **272**, 113936.
16 A. A. Farooqi, R. Attar, U. Y. Sabitaliyevich, N. Alaaeddine, D. P. de Sousa, B. Xu and W. C. Cho, *Cancers*, 2020, **12**.
17 J. C. W. Lim, T. K. Chan, D. S. Ng, S. R. Sagineedu, J. Stanslas and W. F. Wong, *Clin. Exp. Pharmacol. Physiol.*, 2012, **39**, 300–310.
18 S. K. Mishra, S. Tripathi, A. Shukla, S. H. Oh and H. M. Kim, *Front. Biosci.*, 2015, **7**, 255–266.
19 S. G. S. Kandanur, S. Nanduri and N. R. Golakoti, *Bioorg. Med. Chem. Lett.*, 2017, **27**, 2854–2862.
20 S. G. S. Kandanur, S. Kundu, C. Cadena, H. S. Juan, A. Bajaj, J. D. Guzman, S. Nanduri and N. R. Golakoti, *Chem. Pap.*, 2019, **73**, 1669–1675.
21 S. G. S. Kandanur, N. R. Golakoti and S. Nanduri, *Bioorg. Med. Chem. Lett.*, 2015, **25**, 5781–5786.
22 N. Tamang, C. Andrews, S. K. Mavileti, S. Nanduri, N. R. Golakoti and B. Karanam, *New J. Chem.*, 2022, **46**, 9745–9754.
23 B. Karanam, N. Tamang, Y. Inabathina, S. K. Mavileti, L. Sripada, S. Nanduri and N. R. Golakoti, *Cancer Res.*, 2023, **83**, 3818.
24 V. Kumar, K. Kaur, G. K. Gupta and A. K. Sharma, *Eur. J. Med. Chem.*, 2013, **69**, 735–753.
25 M. Faisal, A. Saeed, S. Hussain, P. Dar and F. A. Larik, *J. Chem. Sci.*, 2019, **131**, 70.
26 A. Ansari, A. Ali, M. Asif and Shamsuzzaman, *New J. Chem.*, 2016, **41**, 16–41.
27 D. E. V. Pires, T. L. Blundell and D. B. Ascher, *J. Med. Chem.*, 2015, **58**, 4066–4072.

Open Access Article. Published on 22 August 2024. Downloaded on 3/8/2026 10:43:55 AM.
This article is licensed under a Creative Commons Attribution-NonCommercial 3.0 Unported Licence.

28 A. Kar, D. Jain, S. Kumar, K. Rajput, S. Pal, K. Rana, R. Kar, S. K. Jha, N. Medatwal, P. S. Yavvari, N. Pandey, D. Mehta, H. Sharma, D. Bhattacharya, M. K. Pradhan, R. D. Sharma, A. Srivastava, U. Agrawal, A. Mukhopadhyay, S. Sengupta, V. S. Patil, A. Bajaj and U. Dasgupta, *Sci. Adv.*, 2023, **9**, 1–22.
29 M. Beniwal and N. Jain, *J. Heterocycl. Chem.*, 2019, **56**, 2508–2516.
30 L. You, Xu Qidong, Z. Xiaoli, Li Shiduo, Z. Hui, B. Wei Wu; X. Liu; L. Li; G. Xin; Z. Jiang and W. Xiaoke, *China Pharmaceutical University, CN115960047A*, 2023.
31 D. L. Pavia, G. M. Lampman and G. S. Kriz, *Introduction to Spectroscopy-A Guide for Students of Organic Chemistry*, Thomson Learning, Inc., 2001.
32 D. L. B. R. M. Silverstein, F. X. Webster and D. J. Kiemle, *Spectrometric Identification of Organic Compounds*, 8th edn, Wiley, 2014.
33 E. Miller, ed. S. P. Langdon, Humana Press, Totowa, NJ, 2004, pp. 191–202.
34 G.-Y. Liou and P. Storz, *Free Radical Res.*, 2010, **44**, 479–496.
35 A. Ganesan, *Curr. Opin. Chem. Biol.*, 2008, **12**, 306–317.

 © 2024 The Author(s). Published by the Royal Society of Chemistry